Optimization a structure of MEMS based PDMS ferroelectret for human body energy harvesting and sensing

Junjie Shi[1], Zhenhua Luo[2], Zhu Dibin[3] and Steve Beeby[1]

[1] Department of Electronics and Computer Science, University of Southampton, United Kingdom

[2] School of Water, Energy and Environment, Cranfield University, United Kingdom

[3] Energy Harvesting Research Group College of Engineering, Mathematics and Physical Sciences, University of Exeter, United Kingdom

E-mail: spb@soton.ac.uk

Abstract

A ferroelectret is typically a charge-storing cellular foam that demonstrates excellent piezoelectric properties making them potentially suitable for both sensing and energy harvesting applications. In this work we developed a numerical finite element analysis (FEA) model to describe ferroelectret materials and to further improve their piezoelectric properties. Using this FEA model, ferroelectret materials with rectangular and parallelogram void structure were designed and then fabricated by casting polydimethysiloxane (PDMS) in microfabricated silicon moulds. The piezoelectric properties and energy harvesting output of the fabricated PDMS ferroelectrets were both simulated and evaluated experimentally. For a single layer PDMS parallelogram void structure, the predicted piezoelectric coefficient d_{33} from the ANSYS simulations is around 320 pC N^{-1}. The fabricated PDMS ferroelectret has a low Young's modulus of 670 kPa and a piezoelectric coefficient of 240 pC N^{-1}. A maximum d_{33} of 520 pC N^{-1} was observed in a multilayer ferroelectret structure. When applying compressive forces simulating a footstep, the material demonstrated an output power of 2.73 μW when connected to a 65 MΩ resistive load.

Keywords: energy harvesting, PDMS ferroelectret, MEMS fabrication

1. Introduction

Piezoelectric materials can be used in the direct mode as sensors or as energy harvesting materials to convert mechanical energy into electrical energy and also as actuators that converts electrical energy into mechanical energy [1–3]. Applications in energy harvesting include converting energy from human movement making piezoelectric materials a potential power source for wearable devices and electronic textiles (e-textiles). In the past, research has focused on the conventional piezoelectric materials such as lead zirconate titanate (PZT), PZT based materials, polyvinylidene fluoride (PVDF) and P(VDF-TrFE) copolymer [4–7]. PZT possesses excellent dielectric and piezoelectric properties, but is a rigid ceramic with a very high Young's modulus (63 GPa), making it unsuitable for wearable applications [8]. In contrast, PVDF is a soft polymer with low Young's modulus (2.9 GPa), but its piezoelectric charge coefficient d_{33} is an order of magnitude lower than of PZT (20 pC N^{-1}) [9]. In addition, the energy harvesting capability is not solely determined by d_{33}, it also effected by permittivity of the material. The low permittivity result in high figure of merit ($d_{33}{}^{*}g_{33}$) can enhanced the energy harvesting capability. Therefore, there is a requirement to develop a compliant piezoelectric material with high levels of piezoelectric activity, low young's modulus and low permittivity suitable for wearable applications.

Ferroelectrets are materials (typically a cellular polymer foam) that store charge across its internal voids and that

exhibits piezoelectric properties [8]. The typical internal structure of a ferroelectret foam is randomly arranged cellular voids with positive and negative charges trapped on opposite on each surfaces of the void. A macroscopic dipoles moment is formed by the separated charges resulting in piezoelectric-like property of ferroelectret. Due to the low elastic modulus of the ferroelectret material, the electrically charged voids undergo large deformation when compressed, the dipole moment of the ferroelectret is reduced; and the electrical filed in the internal voids is compensated by net charges which are generated on the electrodes on the outer surfaces of the ferroelectret material. A commercial polypropylene (PP) foam ferroelectret has a d_{33} of 250–400 pC N^{-1}, which is comparable to the d_{33} of bulk ceramic PZT (300–650 pC N^{-1}). The piezoelectric properties of a ferroelectret are dependent on the structure of the cellular voids, the material characteristics and the amount of charge trapped on the void surfaces [10–12].

Most ferroelectrets foams are produced using a blow and extrusion process on polymer films [13–15]. The individual void geometry and overall cellular structure of the ferroelectret foam are typically ill-controlled due to the stochastic nature of these fabrication processes. It is anticipated that the piezoelectric properties of a ferroelectret material can potentially be improved by optimising its internal structure. A number of previous works have attempted to control the geometry of the ferroelectret's internal voids. Wang *et al* [16] used a Su-8 photoresist mould on a silicon wafer to fabricate a polydimethylsiloxane (PDMS) ferroelectret with 50 × 50 × 50 μm^3 size cubic internal voids. This approach provided control over the dimensions of the internal voids in the ferroelectret but did not consider the effect of the geometry of the individual voids on the resulting piezoelectric properties. The demonstrated piezoelectric coefficient d_{33} was 182 pC N^{-1}, for the pure PDMS structure, which was about 40% smaller than the PP foam ferroelectret. A similar mould-casting approach fabricated PDMS ferroelectret with circular voids with a diameter of 100 μm and height of 40 μm [17]. The d_{33} of the fabricated ferroelectret was 350 pC N^{-1}. However, the cross sectional geometry of the fabricated ferroelecteret is still rectangular shape, the other types of cross sectional geometry of the voids was also not modelled in this work.

In our previous work, we demonstrated the optimisation of a PDMS structure based on rectangular void for human body energy harvesting [18]. In this work, the numerical model has been applied to explore the effect of the microscale dimensions and a variety of void geometry on the properties of the ferroelectret. Based on this model, PDMS ferroelectrets with various void structures have been fabricated using silicon casting moulds made by MEMS fabrication techniques. This paper presents a summary of the theoretical predictions and the comparison of the simulations against the experimental results. An improved void structure of PDMS ferroelectret has been proposed using the model.

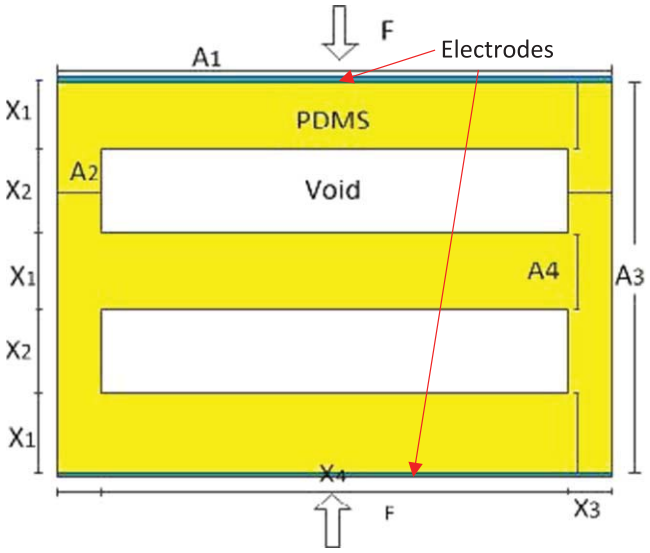

Figure 1. A simplified model for the piezoelectric properties of a charge-implanted cellular structure (x_1 and x_2 are the thickness of the solid and void layers, respectively; A_1 and A_2 are the areas of the solid and void layers in horizontal direction, respectively; A_3 and A_4 are the areas of the solid and void layers in vertical direction, respectively; F represents the external force applied to the outer surface of the material) [19].

2. Numerical algorithm and simulation

To analyse the piezoelectric properties of a ferroelectret, a simplified model for a charge implanted cellular PDMS structure with micrometre-sized voids is illustrated in figure 1 [18, 19].

For a structure with n void layers and $n + 1$ solid layers, the electric field in the solid layers (E_1) and void layers (E_2) can be obtained from Gauss' law for the interfaces:

$$E_1 = \frac{\sigma_m}{\varepsilon_1 \varepsilon_0} \text{ and } E_2 = \frac{\sigma_m - \sigma}{\varepsilon_2 \varepsilon_0}, \tag{1}$$

where σ_m is the charge density on the electrodes, σ is the charge density on the void surface, and ε_0, ε_1 and ε_2 are the vacuum permittivity, the relative dielectric constant of PDMS and the relative dielectric constant of air ($\varepsilon_2 = 1$), respectively.

From Kirchhoff's second law for short circuit conditions:

$$V = \int E \, \mathrm{d}x = (n + 1)x_1 E_1 + n x_2 E_2 = 0, \tag{2}$$

where V is the electric potential across the electrode pair, and x_1 and x_2 are the thickness of the solid and void layers, respectively.

It is found that:

$$\sigma_m = \frac{n\varepsilon_1 \sigma x_2}{[(n + 1)x_1 + n\varepsilon_1 x_2]}. \tag{3}$$

Therefore, the variation of the charge density on the electrodes ($\Delta\sigma_m$) can be expressed as a function of the thickness

variation (Δx_1 and Δx_2) by:

$$\Delta\sigma_m = \frac{\partial\sigma_m}{\partial x_1}\Delta x_1 + \frac{\partial\sigma_m}{\partial x_2}\Delta x_2 = \frac{-n(n+1)\varepsilon_1\sigma x_2}{[(n+1)x_1 + n\varepsilon_1 x_2]^2}$$
$$\Delta x_1 + \frac{n(n+1)\varepsilon_1\sigma x_1}{[(n+1)x_1 + n\varepsilon_1 x_2]^2}\Delta x_2. \quad (4)$$

When an external force (F) deforms the multilayer structure, the relationships between the resulting stresses and strains can be expressed as:

$$\frac{F}{A_3} = c_{33}\frac{\Delta x_3}{x_3} \text{ and } \frac{F}{A_4} = \frac{F}{sr_2 A_3} = c_{33}\frac{\Delta x_4}{x_4}, \quad (5)$$

where c_{33} is the elastic modulus of PDMS, A_3 and A_4 are the areas of the solid and void layers, respectively and sr_2 is the ratio of A_4 to A_3.

The relationship between the thickness variations, Δx_3 and Δx_4, is therefore:

$$\frac{\Delta x_4}{\Delta x_3} = \frac{1}{sr_2}\frac{x_4}{x_3} = \frac{tr_2}{sr_2}, \quad (6)$$

where tr_2 is the ratio of x_4 to x_3, Due to the Poisson effect, the relationships between the thickness variations, Δx_3 and Δx_2, Δx_4 and Δx_1, are therefore:

$$\gamma\frac{\Delta x_3}{x_3} = \frac{\Delta x_2}{x_2} \text{ and } \gamma\frac{\Delta x_4}{x_4} = \frac{\Delta x_1}{x_1}, \quad (7)$$

where γ is the Poisson's ratio, By substituting equation (6) into (7), the relationship between Δx_2, Δx_1, x_2 and x_1 is therefore:

$$\Delta x_1 x_2 = \frac{1}{sr_2}\Delta x_2 x_1. \quad (8)$$

By substituting equation (8) into (4), the variation of the charge density on the electrodes ($\Delta\sigma_m$) can be expressed as:

$$\Delta\sigma_m = \frac{n(n+1)\varepsilon_1\sigma(sr_2 - 1)x_2}{[(n+1)x_1 + n\varepsilon_1 x_2]^2}\Delta x_1. \quad (9)$$

Since only a certain portion of the electrode surface is charged, the effective charge density $(\sigma_m)_{\text{eff}}$, and its variation, $(\Delta\sigma_m)_{\text{eff}}$, should be:

$$(\sigma_m)_{\text{eff}} = (1 - sr_1)\sigma_m \text{ and } (\Delta\sigma_m)_{\text{eff}} = (1 - sr_1)\Delta\sigma_m, \quad (10)$$

where A_1 and A_2 are the effective areas of the solid and void layers, respectively, and sr_1 is the ratio of A_2 to A_1.

By its definition, the piezoelectric coefficient (d_{31}) can be expressed as:

$$d_{31} = \frac{(\Delta\sigma_m)_{\text{eff}}}{F/A_3} = \frac{n(n+1)\varepsilon_1\sigma tr_1(1 - sr_1)(sr_2 - 1)\gamma}{[(n+1) + n\varepsilon_1 tr_1]^2 c_{33}}, \quad (11)$$

where tr_1 is the ratio of x_2 to x_1, Because the piezoelectric coefficient (d_{33}) can be expressed as:

$$d_{33} = \frac{(\Delta\sigma_m)_{\text{eff}}}{F/A_1} = \frac{n(n+1)\varepsilon_1\sigma tr_1(1 - sr_1)^2}{sr_1[(n+1) + n\varepsilon_1 tr_1]^2 c_{33}}. \quad (12)$$

Hence,

$$\frac{d_{33}}{d_{31}} = \frac{1 - sr_1}{sr_1(sr_2 - 1)\gamma} \ (0 < sr_1, sr_2 < 1). \quad (13)$$

Because n, ε_1 and tr_1 are always positive:

$$(n+1) + n\varepsilon_1 tr_1 \geqslant 2\sqrt{n(n+1)\varepsilon_1 tr_1\varepsilon_1}. \quad (14)$$

The piezoelectric coefficient (d_{33}) can be simplified as:

$$d_{33} \leqslant \frac{(1 - sr_1)^2\sigma}{4sr_1 c_{33}} (0 < sr_1 < 1). \quad (15)$$

According to equation 12, the piezoelectric properties of a charged implanted, cellular polymer structure is determined by its geometry, elastic modulus and charge density. Since the elastic modulus and charge density of PDMS are constants in this work, the geometry of void can be investigated and its influence on the piezoelectric properties of the ferroelectret explored.

The mathematical analysis in equations (1)–(15) is only suitable for the basic rectangular voids shown in figure 1. More complex void geometries can be approximated to equivalent rectangles or must be simulated using FEA software to determine the void displacements. In order to investigate the effect of void geometry on void displacement, a rectangular, parallelogram, sector and isosceles trapezium geometries have been modelled (figure 2). These were chosen because they can be arranged to have identical void areas (A_2), area ratio sr_1 and thickness ratio tr_1. The parallelogram, sector and isosceles trapezium void shapes were modelled as equivalent rectangles (shown in figure 2) and were simulated in ANSYS 2D. The overall three-dimensional structures for the four geometries are shown in figure 3.

All structures of PDMS are simulated in ANSYS 2D model, figure 4(a) shows the 2D FEA mesh for the rectangular structure. Each structure was subjected to an external compressive mechanical load through the thickness of the material and ANSYS simulation used to determine the theoretical deformation of the voids. Assuming the charge density on the void surface is uniform, the variation in the net charge developed on the external surface can be calculated from the average deformation. In this case, the piezoelectric coefficient d_{33} can be estimated by:

$$d_{33} = \frac{(\Delta\sigma_m)_{\text{eff}}}{F/A_1}. \quad (16)$$

By substituting equation (4) into (16), the piezoelectric coefficient d_{33} can be expressed as

$$d_{33} = 2\varepsilon_1\sigma_m(x_2\Delta x_1 + x_1\Delta x_2)(2x_1 + \varepsilon_1 x_2)^{-2}P^{-1}, \quad (17)$$

where Δx_1 and Δx_2 are the average variations of the thickness due to the applied external pressure P calculated as shown in figure 4(b). The theoretical d_{33} values for the 4 geometries calculated from the FEA (equation (17)) were compared with the results from the equivalent rectangle model, as shown in figure 5.

When the void is rectangular, figures 5(a) and (b) shows that the d_{33} increases significantly with the decreasing of sr_1 when $tr_1 = 0.8$, and increases slightly with the increasing of tr_1 when $sr_1 = 0.4$. In addition, from these results, there is a difference of 20%–30% between the results from equivalent rectangle model and the ANSYS simulation. The difference is possibly caused by the fact that the analytical model only

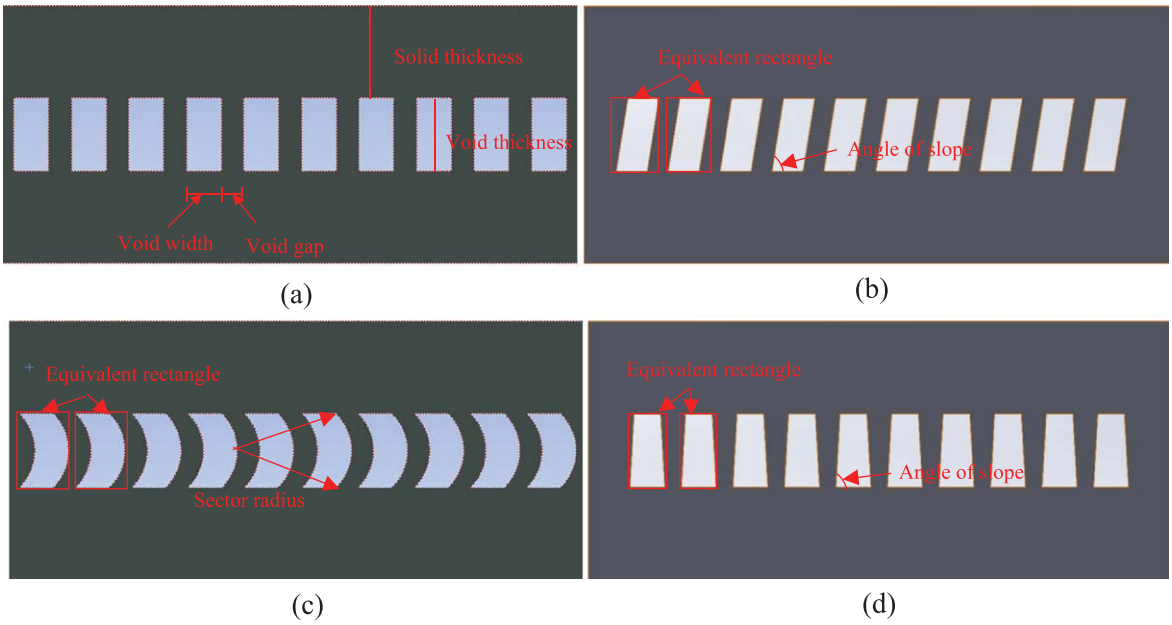

Figure 2. The structure of PDMS ferroelectret models with (a) rectangular voids, (b) parallelogram voids (c) sector shaped voids and (d) isosceles trapezium voids.

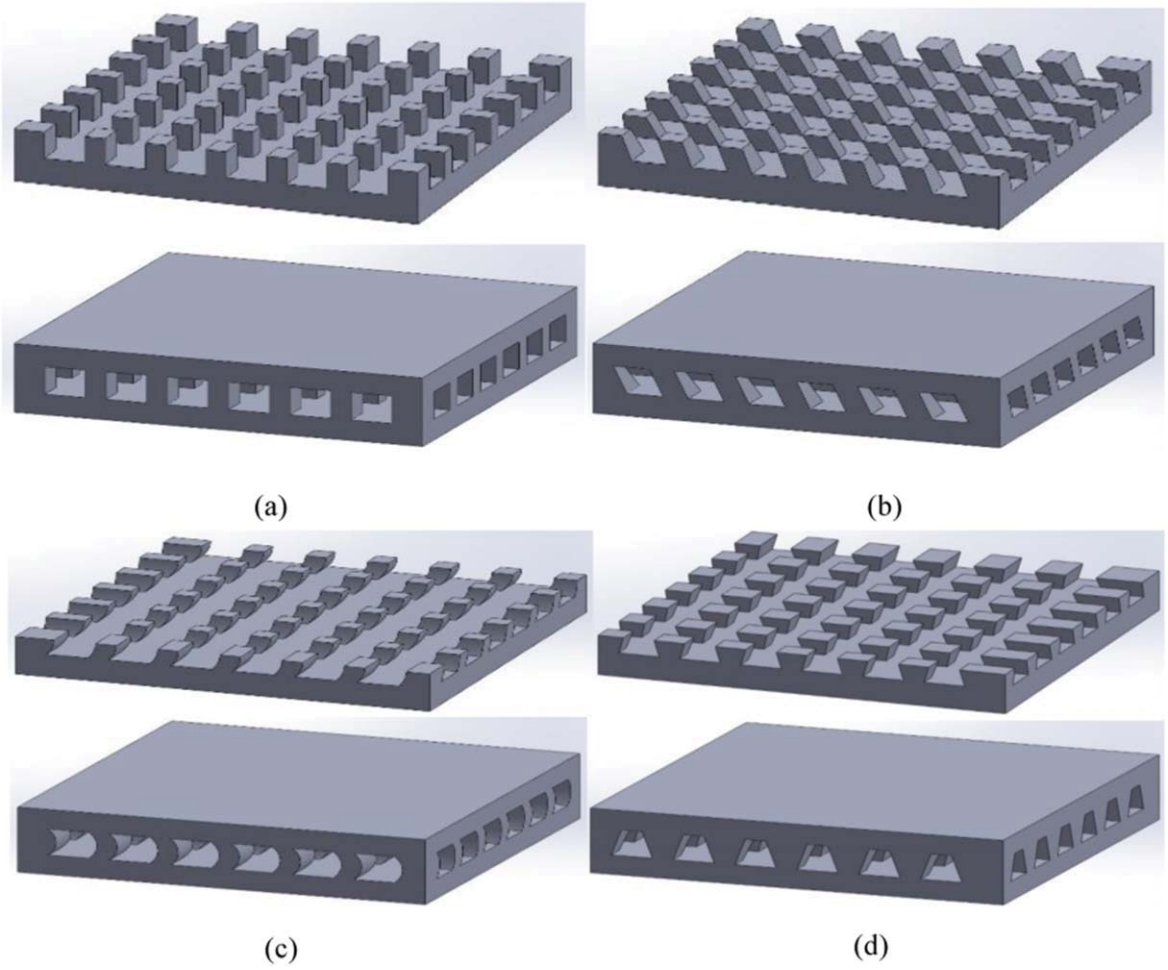

Figure 3. The cross sections and assembled ferroelectrets for (a) rectangular (b) parallelogram (c) sector (d) isosceles trapezium voids.

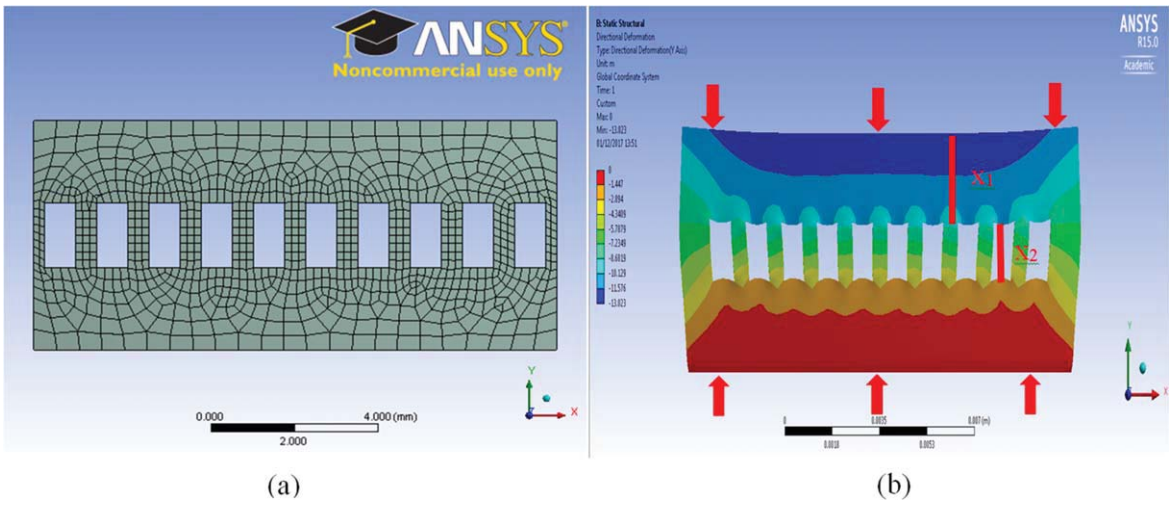

Figure 4. (a) 2D FEA mesh for the rectangular structure; (b) ANSYS simulation deformation results in thickness direction for single layer rectangle void ferroelectret.

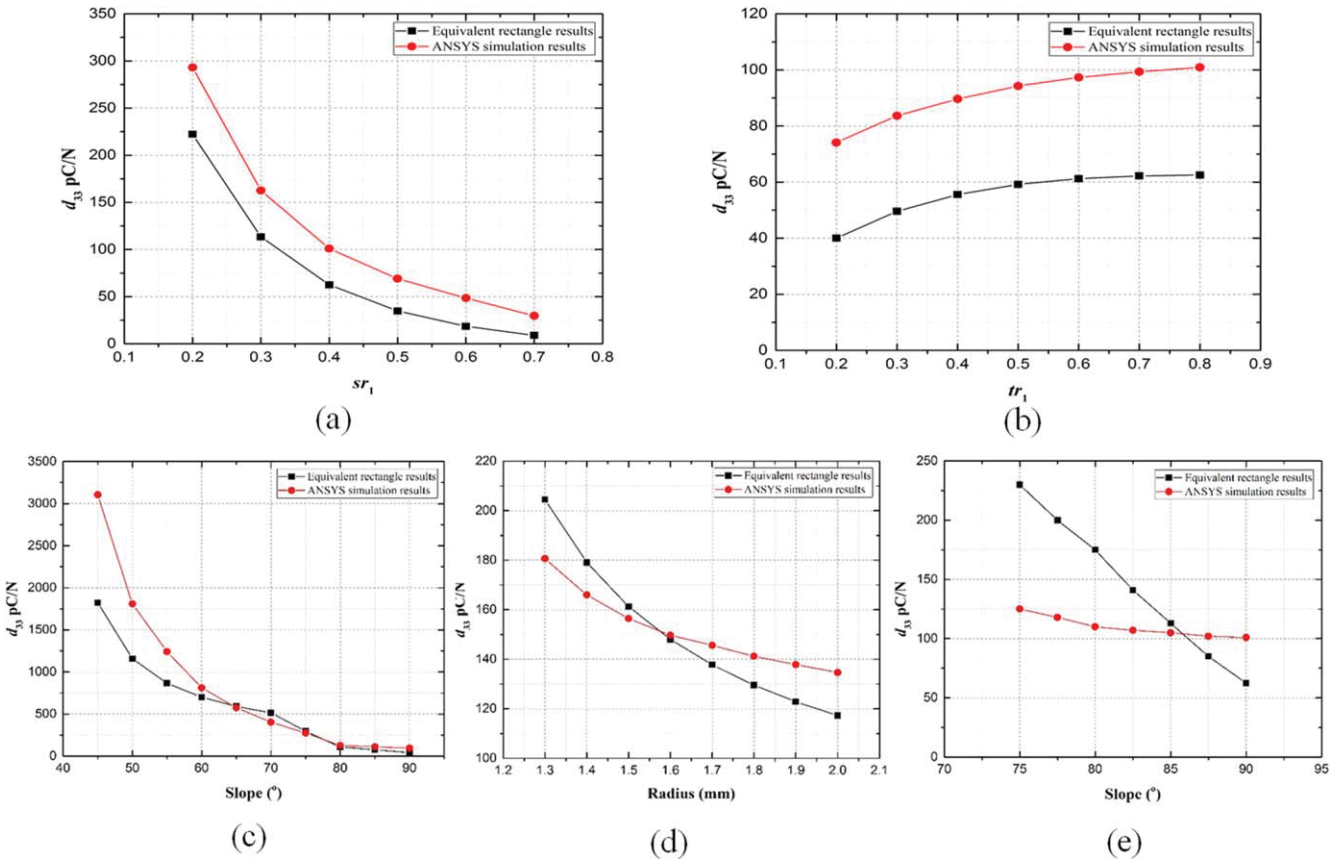

Figure 5. Equivalent rectangle results and ANSYS simulation results for d_{33} from an applied pressure 1 kPa: (a) rectangle voids versus with sr_1 with $tr_1 = 0.8$; (b) rectangle voids versus tr_1 with $sr_1 = 0.4$; (c) parallelogram voids varying with the angle of slope from 45° to 90° with $sr_1 = 0.4$ and $tr_1 = 0.8$; (d) sector voids varying with sector radius with $sr_1 = 0.4$ and $tr_1 = 0.8$; (e) isosceles trapezium varying with the angle of slope from 75° to 90° with $sr_1 = 0.4$ and $tr_1 = 0.8$.

considers rigid deformation. The analytical model does not take into account any bending deformation of the material, resulting in the shape of void being unchanged.

For the parallelogram void geometry, d_{33} varies with the angle of slope, which is the acute angle between the hypotenuse and the base, as shown in figure 2(b). From figure 5(c), the d_{33} is a maximum at 45° and this reduces with increasing angle until the parallelogram becomes a rectangle. For the sector void geometry, the d_{33} versus radius is shown in figure 5(d), which indicates d_{33} decreases with the increasing sector radius. For the isosceles trapezium void geometry, d_{33} varies with the angle of slope which is defined in figure 2(d).

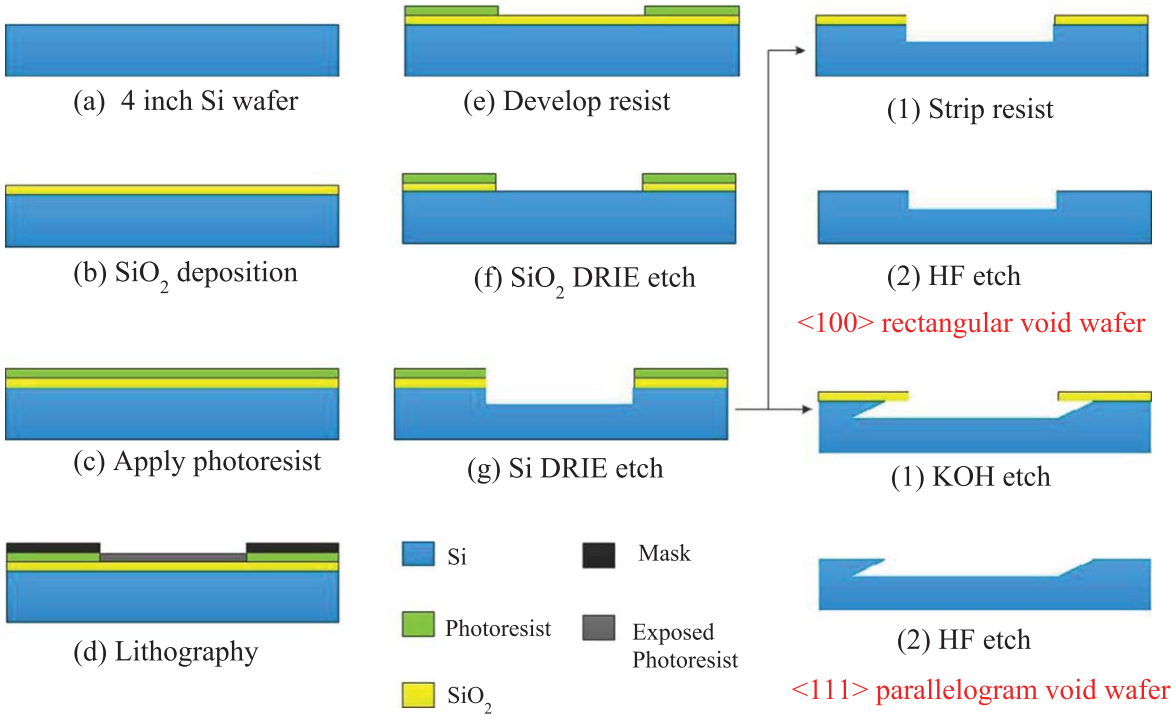

Figure 6. Schematic of silicon mould fabrication processes for ⟨100⟩ rectangular void and ⟨111⟩ parallelogram void wafer.

From figure 5 (e), the d_{33} slightly increase with angle reducing from 90° to 75°. For parallelogram and isosceles trapezium void geometry, the equivalent rectangle model results show an increasing disagreement with the ANSYS simulation results as the angle of the slope decreases. Of these four void geometries, the parallelogram void ferroelectret can achieve higher piezoelectric d_{33} coefficient.

3. Fabrication

Due to Paschen's law, scaling down the thickness of the ferroelectret is a possible approach to enhancing the internal void surface charge density resulting in improved the piezoelectric coefficients d_{33}. The moulds used to fabricate the microscale rectangular and parallelogram voids were fabricated from silicon wafers using a bulk micromachining process, as shown in figure 6. The rectangular mould was fabricated from a ⟨100⟩ wafer whilst the parallelogram mould used a ⟨111⟩ wafer. A layer of 2 μm thick silicon dioxide was deposited on a blank silicon wafer by plasma-enhanced chemical vapour deposition (PECVD). Next, a 5 μm thick of photoresist (AZ9260) was spin-coated on the silicon dioxide layer and then baked on a hotplate at 110 °C for 120 s. The mould pattern was defined using standard contact lithography with a 10 s exposure followed by development in AZ400K for 6 min An inductively coupled plasma etch was used to etch the exposed silicon dioxide and this was followed by stripping the resist leaving the patterned silicon dioxide masking layer. The wafer then dip etched in hydrofluoric acid (HF) to remove the natural silicon dioxide and the silicon was deep reaction ion etched (DRIE) to a depth of 50 μm. On the ⟨100 wafer this formed the rectangular mould and the process is completed by stripping the remaining silicon dioxide. For the ⟨111⟩ wafer, the parallelogram structure was formed by following the DRIE etch with a wet anisotropic potassium hydroxide (KOH) etch. The anisotropic nature of the etch converts the rectangular structure into a parallelogram cross-section with an angle of slope of 70.5° as defined by the crystalline planes [20]. The top view of the fabricated rectangular and parallelogram moulds are shown in figures 7(a) and (b), respectively. The cross-section view of the fabricated rectangular and parallelogram void silicon mould are shown in figure 7(c).

To experimentally evaluate the piezoelectric properties of the ferroelectret at different area ratios, three rectangular and parallelogram void structures with area ratios of 0.25, 0.16 and 0.0625 were explored. Silicon moulds with three different depths (30/40/50 μm) were fabricated to evaluate the effect of the thickness ratio. A summary of the main parameters of the fabricated samples is shown in table 1.

The PDMS layer was fabricated by mixing a liquid PDMS and curing agent (Sylgard 184 from Dow Corning, MI, USA) at a ratio of 10:1 by weight and then degassed in a vacuum desiccator. To remove the moisture on the mould, the wafer was cleaned by acetone and oven baked for 15 min at 120 °C. A thin PDMS mixture layer was spin-coated on the silicon wafer mould and cured for 1 h at 80 °C. The thickness of the PDMS membrane was controlled by the speed and duration of the spin-coating [21]. For this experiment, the duration of spin-coating was fixed at 30 s. To achieve the designed thickness ratio, a summary of the spin-coating speeds is listed in table 2. The mould was immersed in water and the finished thin PDMS membrane was peeled away from

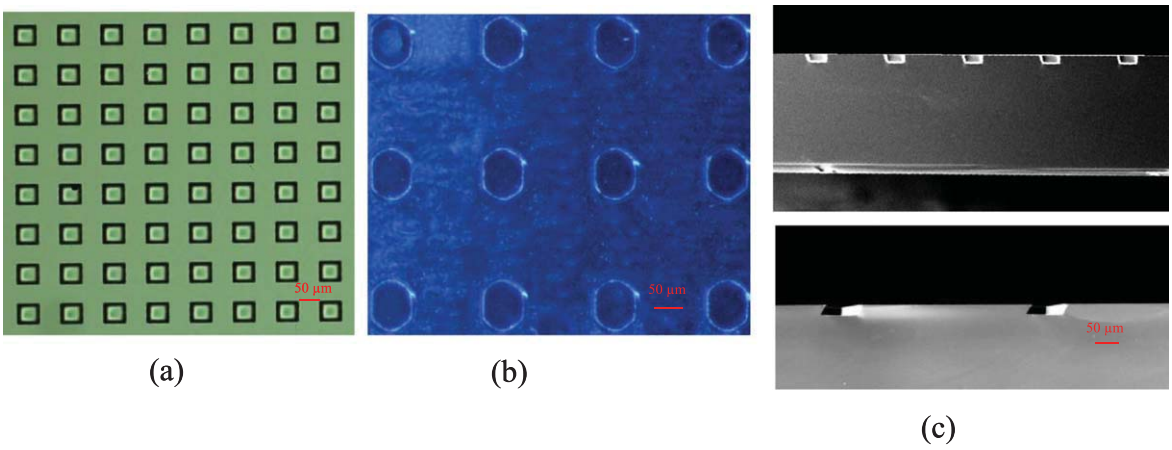

Figure 7. (a) The optical microscope image of top view of the fabricated rectangular mould; (b) the optical microscope image of top view of the fabricated parallelogram mould; (c) the SEM image of cross-section view of fabricated rectangular and parallelogram void silicon mould.

Table 1. A summary of the parameters the fabricated ferroelectret.

Void shape	tr_1	sr_1	Void thickness (μm)	Void width (μm)	Void gap (μm)
Rectangular	0.4–0.8	0.25/0.16/0.0625	30/40/50	50/75/150	50
Parallelogram	0.4–0.8	0.25/0.16/0.0625	30/40/50	46.3/71.3/146.3	53.7

Table 2. A summary of the speed of the spin coating.

Void thickness	30 μm	40 μm	50 μm
0.4	1145 rpm	890 rpm	730 rpm
0.5	1390 rpm	1080 rpm	890 rpm
0.6	1630 rpm	1270 rpm	1045 rpm
0.7	1870 rpm	1450 rpm	1195 rpm
0.8	2100 rpm	1630 rpm	1340 rpm

the mould. This process was repeated using a plain unetched silicon wafer to produce an unstructured smooth PDMS layer. Both PDMS films were then given an oxygen plasma treatment (Femto Asher, Diener, Germany, 30 S at 35–40 W). Immediately after the plasma treatment, the two PDMS layers were bonded together by applying a gentle pressure. The bonded PDMS assembly was baked in oven at 80 °C for 1 h to improve the bond strength [22]. Multi-layered samples were constructed by repeating the processes.

The fabricated PDMS samples (2 cm × 2 cm) were corona charged, which generated macroscopic dipoles by the gas-breakdown inside the voids during charging. The corona charging needle was located with its tip about 3–4 cm above the sample surface. The PDMS was charged with a needle voltage of −25 kV for 2 min at room temperature. The external electrodes were formed using adhesive silver tape.

Figures 8 and 9 show the cross-section image of the fabricated ferroelectret membranes with rectangular and parallelogram voids, and the multilayer structures, respectively. From these figures, it can observed that the designed void shape was successfully fabricated and have excellent uniformity. However, it found that the voids are not aligned vertically in the multilayer ferroelectrets.

4. Experimental validation

4.1. Experimental step

To experimentally validate the simulated results, rectangular and parallelograms voids with the same effective area ratio were fabricated using the silicon moulds. The top view of the rectangular and parallelogram void structures were square-shaped and hexagon-shaped, respectively (figure 7). In order to achieve the same effective area ratio, the area of hexagon should be equal to the area of the square.

To investigate the energy harvesting performance of the PDMS ferroelectret, the experiment was carried on immediately after polarizing the samples. An Instron electrodynamic instrument (EletroPuls E1000, Instron Ltd) was used to apply a repeatable force profile that simulates the forces applied during walking. The average step frequency of a human walking is in the range of 0.4–1.45 step per second [23–25]. Three compressive force profiles were applied with a maximum force of 800 N and their waveforms are shown in figure 10. The output voltages of the PDMS ferroelectret under these compressive forces were recorded using an oscilloscope (TDS2014, Tektronix UK Ltd) for different load resistances from 1 MΩ to 1 GΩ.

4.2. Result and discussion

4.2.1. Piezoelectric coefficients measurement. Results of piezoelectric coefficient d_{33} varying with the thickness ratio for PDMS ferroelectret with one, two and three void layers are shown in figures 11(a)–(c), respectively. The piezoelectric charge constant d_{33} is measured using a PiezoMeter PM300 (Piezotest Ltd). For this measurement, the measurement

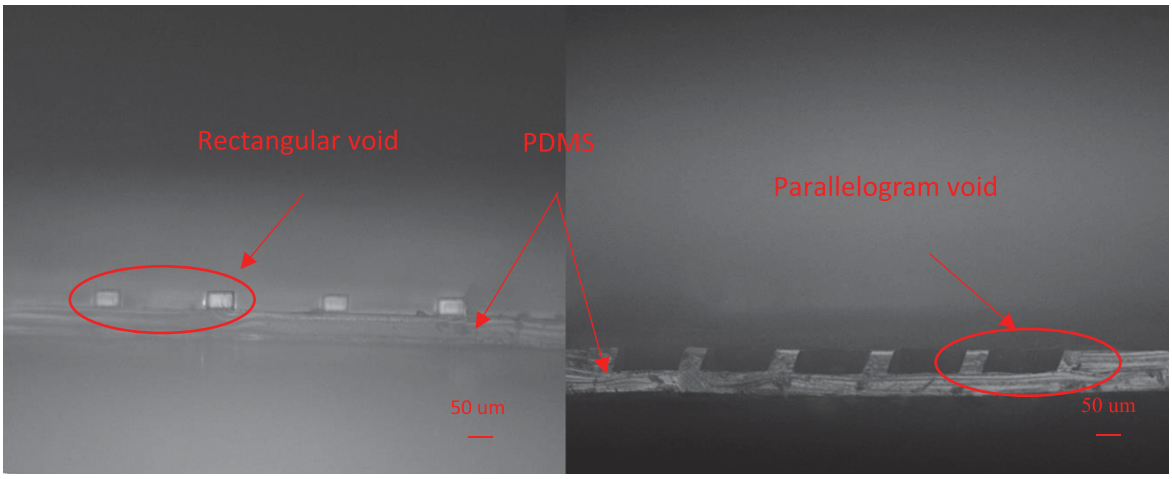

Figure 8. The SEM image of the cross section image for fabricated (a) rectangular void and (b) parallelogram void PDMS ferroelectret membrane.

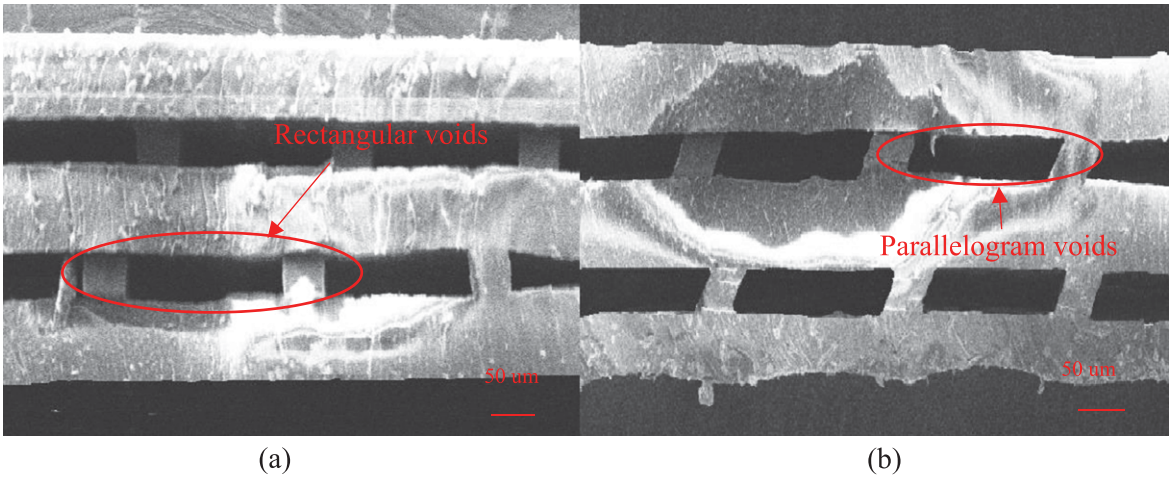

Figure 9. The image of the cross section for multilayer PDMS ferroelectret (a) rectangular PDMS ferroelectret (b) parallelogram void PDMS ferroelectret.

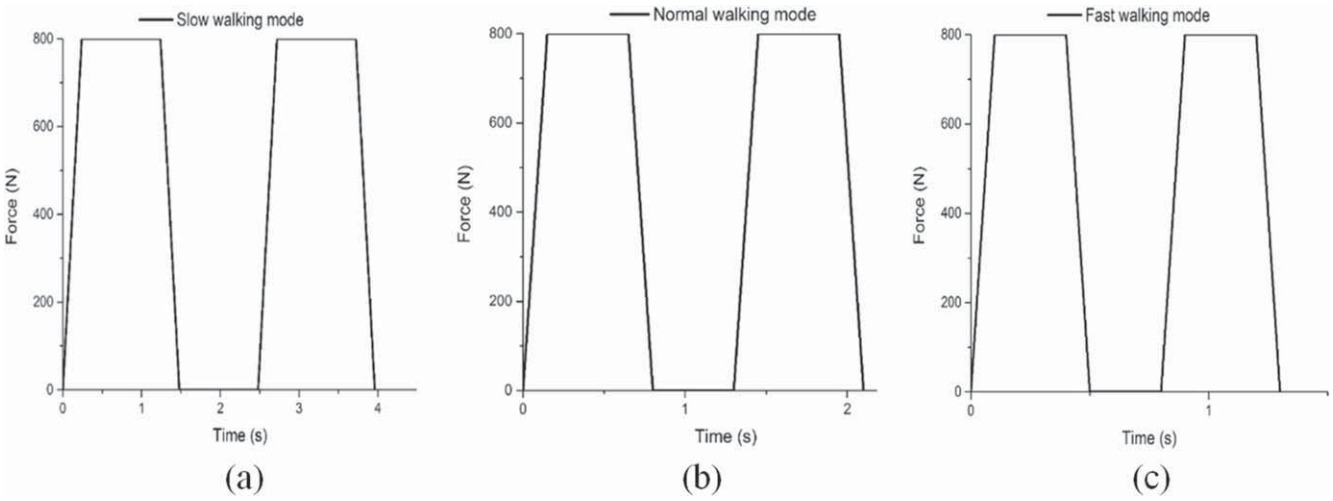

Figure 10. Waveform of applied compressive force at (a) slow walk at 0.4 step s^{-1}: 0.24 s transition time of the applied force from 0 to 800 N and duration of the maximum force was 1 s; (b) medium walking speed at 0.8 step s^{-1}, transition time 0.15 s and duration of the maximum force 0.5 s; (c) fast walk at 1.4 step s^{-1}, transition time 0.1 s, duration of the maximum force 0.3 s.

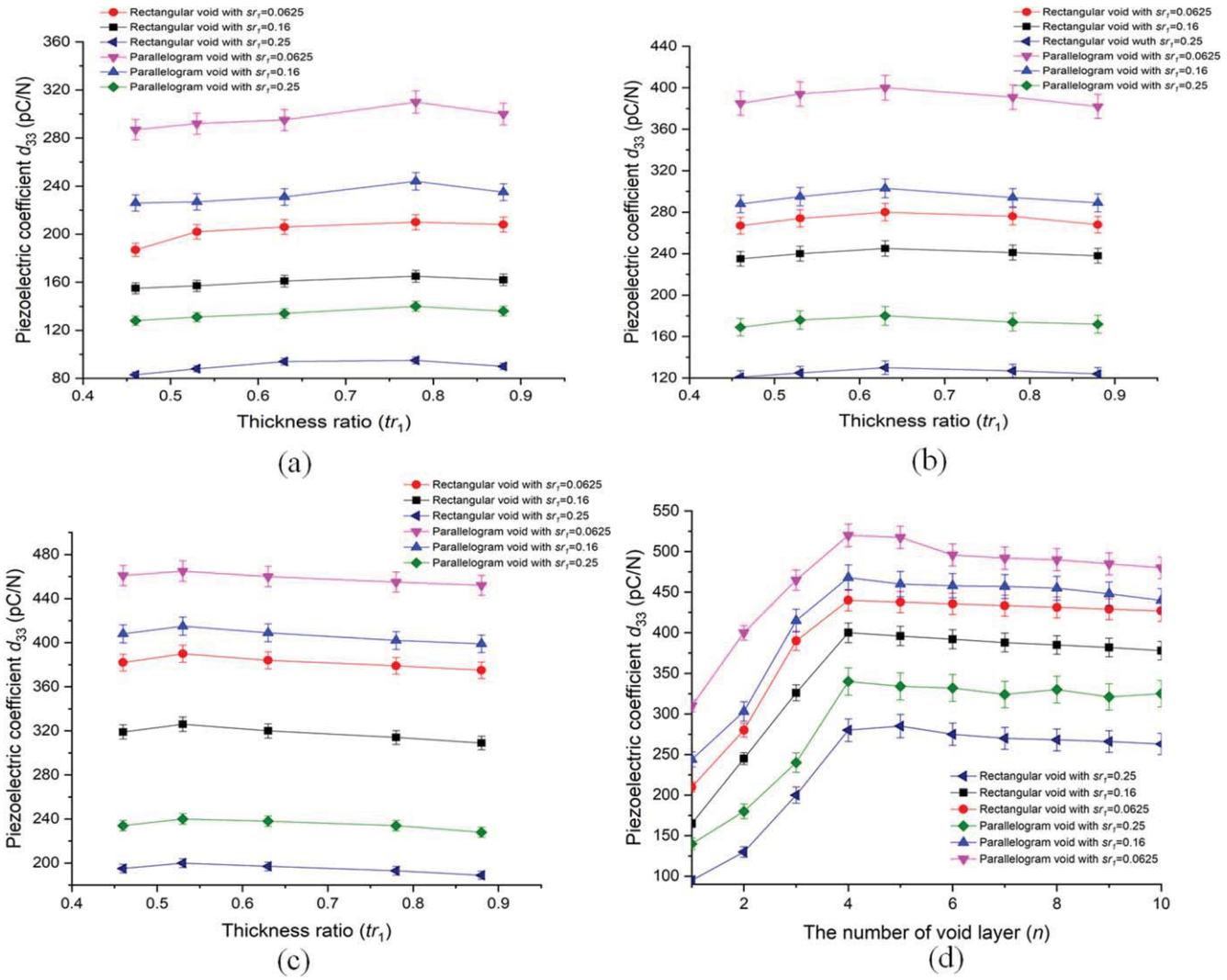

Figure 11. The measured piezoelectric coefficient varying with the thickness ratio for (a) one void layer, (b) two void layers and (c) three void layers; (d) The measured piezoelectric coefficient varying with the number of void layers with optimum tr_1 for each geometry.

setting was a dynamic force of 0.25 N, static force of 10 N and frequency of 110 Hz. It is found that the piezoelectric confident d_{33} of both samples increase with the thickness ratio. The best piezoelectric properties for one, two and three void layers PDMS ferroelectret are achieved around the thickness ratio of 0.8, 0.6 and 0.55, respectively. It is also found that the effective area ratio does affect the resulting piezoelectricity. With the number of void layer increasing, the variations of piezoelectric properties were shown in figure 11(d). When stacking more void layers together up to 4 layers, it is found that d_{33} of PDMS ferroelectret have a significant improvement. The maximum piezoelectric coefficients d_{33} are achieved by 4-layer PDMS ferroelectret, about 520 pC N^{-1}. When 5 or more layers are stacked, d_{33} does not increase any further. This may be due to an increase in Young's modulus of the ferroelectrets as the number of void layers increases, resulting in a decrease in piezoelectricity [26]. Table 3 provides the piezoelectric coefficient values of different ferroelectret material in order to compare them with the fabricated PDMS reported in this work. The fabricated PDMS exhibits an important piezoelectric properties compared to other ones.

Table 3. Piezoelectric coefficient values for piezoelectric polymer materials.

Piezoelectric material	d_{33} (pC N^{-1})	Young's modulus (kPa)
Cellular PDMS (Our current work)	240	670
Cellular PDMS [17]	350	300
Cellular PDMS [19]	32.8	500
Cellular PP [27]	200	1500
PTFE/FEP multilayer VCP [28]	300	2400

For ANSYS simulation results, the predicted piezoelectric coefficient d_{33} of rectangular and parallelogram one void layer PDMS ferroelectret with $sr_1 = 0.16$ and $tr_1 = 0.8$ are around 100 and 320 pC N^{-1}, respectively. The experimental d_{33} of the rectangular and parallelogram void single

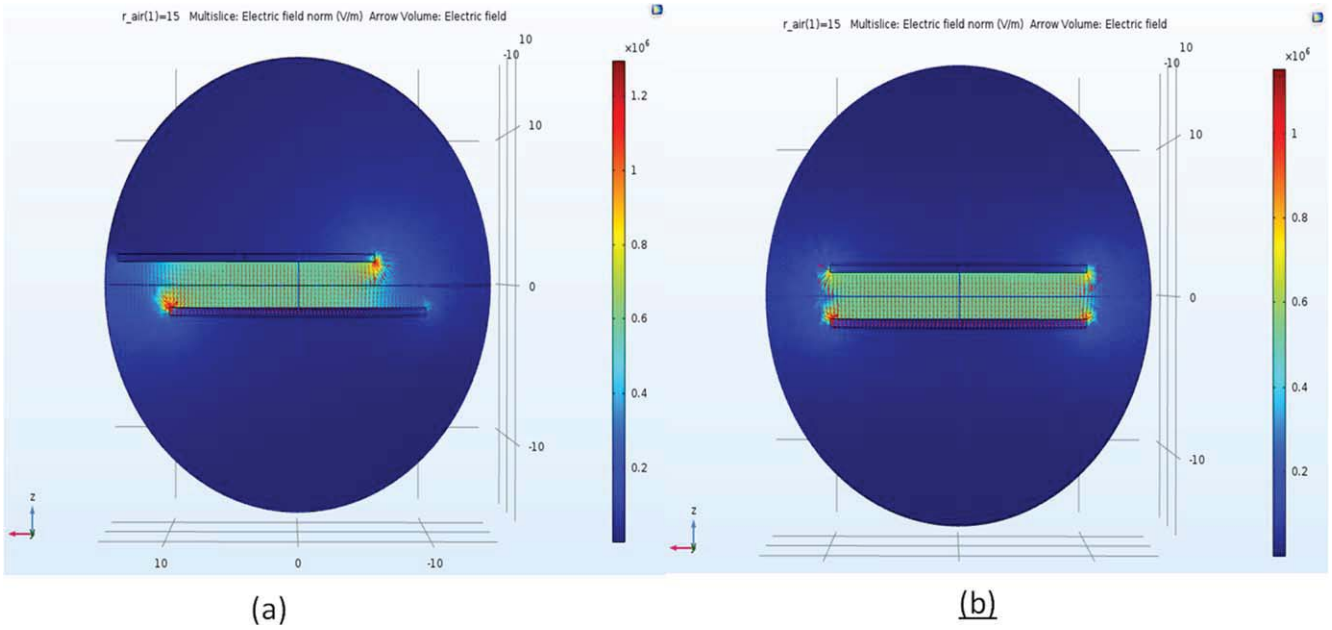

Figure 12. The simulated electric filed distribution for identical charge distribution on (a) parallelogram void and (b) rectangular void.

layer PDMS ferroelectret are 160 and 250 pC N^{-1}, respectively (figure 11(d)). The measured effective elastic modulus is about 670 kPa. Whilst the predicted values may be different, both the simulated and practical results show the parallelogram voids give higher piezoelectric properties than the rectangular voids. The difference between the simulation and experimental results is potentially due to the analytical calculation of d_{33} which assumes identical charge distribution for the parallelogram and rectangular voids. Results of simulated electric field distribution for parallelogram void and rectangular void with identical charge distribution condition are shown in figures 12(a) and (b), respectively. It is found the electric field for the overlapping area of the parallelogram void with the upper and lower siders is uniformly distributed, as same as the electric field distribution of rectangular void. In contrast, the electric field distribution in the region between the ends of the parallelogram void is non-uniformly distributed. In other word, the actual charge distribution in parallelogram void should not be identical. However, the established model is based on the assumption that the internal electric field is evenly distributed. Therefore, the experimental results and theoretical results have certain errors. Also the calculation of area ratio for the parallelogram is identical to the rectangular structure and this may not be as accurate given the sloping sidewalls of the parallelogram structure.

4.2.2. Investigation of energy harvesting performance. Figure 13(a) shows the characteristic current–voltage (I–V) curves of a four layers parallelogram PDMS ferroelectret under compressive forces that were applied in normal walking mode, as a function of load resistance. The voltage values used in figure 13(a) are the average of measured voltages from three consecutive pulses. The peak current decreases with increasing load resistance in the range of 1 MΩ–1 GΩ. The voltage increases with increasing load resistance. Consequently, the power output reaches a maximum value of 2.73 μW with a 65 MΩ loading resistance as shown in figure 13(b). The energy output of the fabricated PDSM ferroelectret is showing output peak power density of 0.68 μW cm^{-2} in normal walking mode. Compared to the commercial pp materials output peak density of 0.34 μW cm^{-2}, there is a significant improvement [29]. Due to impedance matching theory, to maximize the output power, the output impedance should be equal to the input impedance of ferroelectret. The input impedance of the ferroelectret can be simplified as impedance of a capacitor. The input impedance of the ferroelectret can be expressed as:

$$X_c = \frac{1}{2\pi f C_f} = R_L, \tag{18}$$

where X_c is the impedance of the ferroelectret, f is the frequency of the output current, C_f is the capacitance of the ferroelectret and the R_L is the output impedance.

In energy harvesting applications where the energy is extracted in pulses it may be preferable that the power management circuit is self-powered [30], i.e. the generated energy is used straightway and no energy storage is used. The advantage of powering from the input comparing to powering from the system energy storage is that the power management circuit is active only during the energy pulse, and thus the overall quiescent losses are minimized. However, the power losses of the power management circuit are strongly influenced by the supply voltage [26, 31]. Therefore, the high voltage generated by the proposed ferroelectret may not be desirable for the electronic circuit. It may also be desirable to increase the pulse width at the expense of energy content in order to reduce the intermittency, which in itself causes system energy loss during start-up, as shown in [32]. In addition, as many integrated circuits only work safely under a

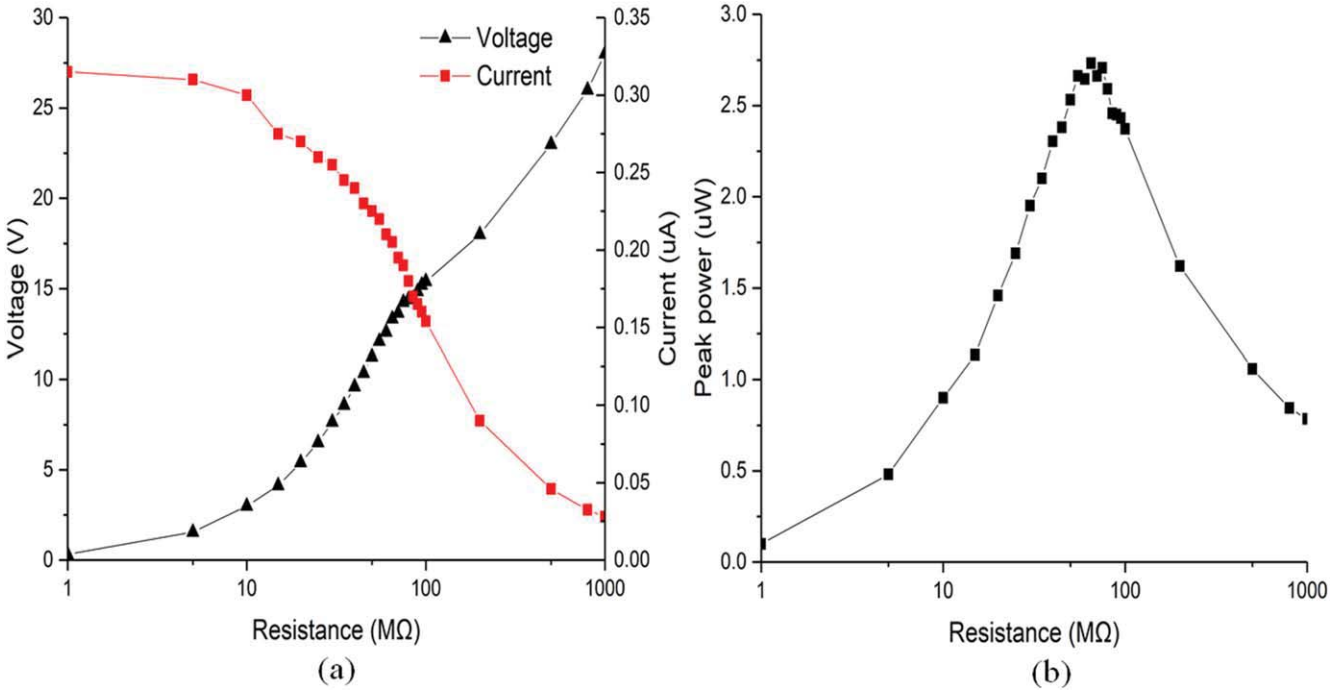

Figure 13. (a) The characteristic *I–V* curves of a four layers PDMS ferroelectret; (b) Instantaneous power output at different resistance loading.

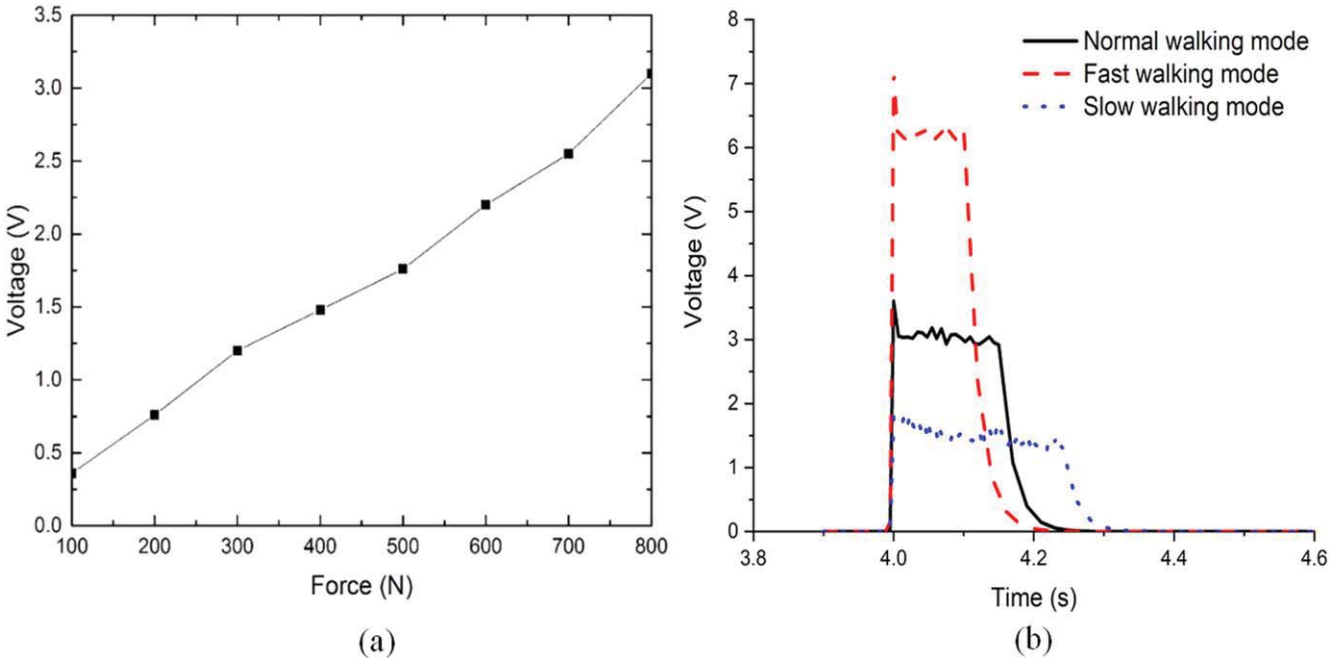

Figure 14. (a) Peak output voltage at different applied compressive forces (b) output voltage pulse for three different model under a constant force of 800 N.

voltage stress of 5.5 V, and a high external resistive load to the materials will make the matching from power converter being difficult in the CMOS process, it is ideal to have output voltage in the range of 1 to 5.5 V. At 10 MΩ, the output peak voltage of the ferroelectret is 3 V and its instantaneous current is 0.3 μA, which, once rectified and smoothed, would be suitable to be used directly as the supply to electronic circuits. Thus 10 MΩ is used as the resistive load in the following measurements.

The maximum compressive force applied on the ferroelectret in this work is set to be 800 N, roughly resembling a walking person with weight of 80 kg in normal walking mode. The energy output is investigated in this work by varying the quantities of compressive forces. Figure 14(a)

shows the change of peak output voltage at different applied forces with load resistance of 10 MΩ. It is found that the output voltage increases linearly with increasing forces.

The output voltage is also affected by the walking mode. Figure 14(b) shows the single output pulses of PDMS ferroelectret under 800 N compressive force in different walking modes. The step frequency of the slow walking mode, normal walking mode and fast walking mode are 0.4 step s^{-1}, 0.8 step s^{-1} and 1.4 step s^{-1}, respectively. From this Figure, the voltage peak increase with the increasing step frequency and the maximum voltage peak is achieved in the fast walking mode with the highest step frequency. However, the duration of voltage output pulses is decreased with the increasing step frequency. This can be explained by considering the change of force. In these walking modes with maximum force of 800 N, the applied compressive force can be considered as an object with a velocity. During the whole collision process, the deformation of sample is regarded as an elasticity deformation. Due to Hooke's law, the applied force on the sample can be expressed as:

$$F = -kX, \tag{19}$$

where F is the applied force, k is a spring constant and X is the deformation of sample.

Thus the force F is directly proportional to X. With the step frequency increasing, the slope of applied force is increasing resulting in increasing deformation of the sample in unit time. As mentioned in previous chapter, the generated charge is directly proportional to the deformation of sample as:

$$V = \frac{\Delta Q}{t}R, \tag{20}$$

where V is the output voltage, ΔQ is the variation of charge, t is the time and R is the load resistance.

For these three walking modes, the applied force are the same resulting in the final deformation of sample should be the same. Thus the amount of variation of charge should be the same. Form equation (20), the peak voltage V of an output pulse is directly proportional to the duration of the applied force. It means that the peak voltage increase with the slope of applied force increasing. This explain the difference in voltage output in different walking modes. For the fast walking mode, it has the shortest transition time of the applied force from 0 to 800 N resulting in the maximum output peak voltage. Comparing with output pulses and the applied force wave function, the duration of output pulses is determined by transition time of the applied force. In addition, with the duration of force holding increasing, the duration of output pulses cannot be enhanced.

5. Conclusions

This paper presents a numerical FEA model to describe ferroelectret materials and to further improve their piezoelectric properties. Based on this FEA model, multilayer ferroelectret material with rectangular and parallelogram void structure were designed and fabricated utilizing silicon fabrication processes. There is a large error between the simulated and measured results, because the FEA software (ANSYS) lack ferroelectret model that can be used directly for predicting the energy performance and output. The FEA model only was used for guiding the design of the ferroelectret structures based on static structural model. However, the practical experiment and numerical results still revealed that the PDMS ferroelectret with lower effective area ratio sr_1 can generate higher piezoelectric coefficients d_{33} and the parallelogram void PDMS ferroelectret based on the same effective area ratio can achieve higher piezoelectric coefficients d_{33} than the rectangular void PDMS ferroelectret. The thickness ratio can also affect the piezoelectric coefficient d_{33}. For one void layer, two void layers and three void layers PDMS ferroelectret, the optimized thickness ratio are achieved around 0.8, 0.6 and 0.55, respectively. When stacking more void layers together up to 4 layers, it is found that d_{33} of PDMS ferroelectret have a significant improvement. The maximum piezoelectric coefficients d_{33} are achieved by 4-layer PDMS ferroelectret, about 520 pC N^{-1}. When 5 or more layers are stacked, d_{33} does not increase any further. This may be due to an increase in Young's modulus of the ferroelectrets as the number of void layers increases, resulting in a decrease in piezoelectricity.

The energy harvesting performance of fabricated PDMS ferroelectrets are also investigated. The parallelogram void PDMS ferroelectret with the maximum piezoelectric coefficients 520 pC N^{-1} and size of 2 cm × 2 cm generates maximally 13 V, 2.73 μW with a 65 MΩ loading under a compressive force of 800 N in normal walking model. It is also found that the output voltage increases linearly with increasing forces. The maximum output voltage peak is affected by the step frequency. In other word, the peak voltage is directly proportional to the slope of applied force. In addition, the duration of output is determined by duration of applied force increasing and cannot enhanced by force holding duration increasing. It means that the static force cannot improve the energy output.

In conclusion, a numerical FEA model for predicting the piezoelectricity of the ferroelectret is developed and briefly verified. The piezoelectricity of the fabricated ferroelectret can be tailored by the adjusting the dimensions of the voids and also effected by the shape of void. The demonstrated PDMS ferroelectret can potentially serve as flexible and wearable electromechanical materials, and fulfils the requirements of a variety of wearable sensor and energy harvesting applications.

ORCID iDs

Junjie Shi https://orcid.org/0000-0001-9440-1902
Zhenhua Luo https://orcid.org/0000-0003-0766-6174
Zhu Dibin https://orcid.org/0000-0003-0517-3974

References

[1] Hindrichsen C C, Lou-Moller R, Hansen K and Thomsen E V 2010 Advantages of PZT thick film for MEMS sensors *Sensors Actuators* A **163** 9–14

[2] Park K-I *et al* 2014 Highly-efficient, flexible piezoelectric PZT thin film nanogenerator on plastic substrates *Adv. Mater.* **26** 2514–20
[3] Hillenbrand J and Sessler G M 2004 High-sensitivity piezoelectric microphones based on stacked cellular polymer films *J. Acoust. Soc. Am.* **116** 3267–70
[4] Heywang W, Lubitz K and Wersing W 2008 *Piezoelectricity: Evolution and Future of a Technology* (Berlin: Springer) vol 114, pp 157–77
[5] Beeby S P, Tudor J M and White N M 2006 Energy harvesting vibration sources for microsystems applications *Meas. Sci. Technol.* **17** R175–95
[6] Erturk A and Inman D J 2011 *Piezoelectric Energy Harvesting* (New York: Wiley) pp 301-324
[7] Radousky H B and Liang H 2012 Energy harvesting: an integrated view of materials, devices and applications *Nanotechnology* **23** 502001
[8] Priya S and Inman D J 2009 *Energy Harvesting Technologies* (Berlin: Springer) pp 3-39
[9] Kazmierski T J and Beeby S 2011 *Energy Harvesting Systems Principles, Modeling and Applications* (Berlin: Springer Science) pp 25-77
[10] Gerhard-Multhaupt R 2002 Less can be more: holes in polymers lead to a new paradigm of piezoelectric materials for electret transducers *IEEE Trans. Dielectr. Electr. Insul.* **9** 850–9
[11] Bauer S, Gerhard-Multhaupt R and Sessler G M 2004 Ferroelectrics: soft electroactive foams for transducers *Phys. Today* **57** 37–43
[12] Hu Z and von Seggem H 2006 Breakdown-induced polarization buildup in porous fluoropolymer sandwiches: a thermally stable piezoelectret *J. Appl. Phys.* **99** 024102
[13] Raukola J 1998 A new technology to manufacture polypropylene foam sheet and biaxially oriented foam films *Dissertation* VTT Publications 361, Technical Research Center of Finland, Tampere University of Technology
[14] Paajanen M, Minkkinen H and Raukola J 2002 Gas diffusion expansion increased thickness and enhanced electromechanical response of cellular polymer electret films *Proc., 11th Int. Symp. on Electrets (Melbourne, Australia , 1–3 October 2002)* (Piscataway, NJ, USA: IEEE Service Center) pp 191–4
[15] Wegener M, Wirges W, Fohlmeister J, Tiersch B and Gerhard-Multhaupt R 2004 Two-step inflation of cellular polypropylene films: void-thickness increase and enhanced electromechanical properties *J. Phys. D: Appl. Phys.* **37** 623–7
[16] Wang J-J, Hsu T-H, Yeh C-N, Tsai J-W and Su Y-C 2012 Piezoelectric polydimethylsiloxane films for MEMS transducers *Micromech. Microeng.* **22** 015013
[17] Kachroudi A, Basrour S, Rufer L, Sylvestre A and Jomni F 2016 Micro-structured PDMS piezoelectric enhancement through charging conditions *Smart Mater. Struct.* **25** 105027
[18] Shi J, Zhu D, Cao Z and Beeby S P 2015 Optimization of a PDMS structure for energy harvesting under compressive forces *J. Phys. Conf. Ser.* **660** 12041
[19] Wang J-J, Hsu T-H, Yeh C-N, Tsai J-W and Su Y-C 2012 Piezoelectric polydimethylsiloxane films for MEMS transducers *J. Micromech. Microeng.* **22** 015013
[20] Wang Y, Li T and Yang H 2013 Nanofabrication, effects and sensors based on micro-electro-mechanical systems technology *Phil. Trans. R. Soc.* A **371** 20120315 (2012)
[21] Koschwanez J H, Carlson R H and Meldrum D R 2009 Thin PDMS films using long spin times or tert-butyl alcohol as a solvent *PLoS One* **4** e4572
[22] Zhang W Y, Ferguson G S and Tatic-Lucic S 2004 Elastomer-supported cold welding for room temperature wafer-level bonding *Micro Electro Mechanical Systems 17th IEEE Int. Conf. on* (MEMS) 741–4
[23] Bertram J E A 2005 Constrained optimization in human walking: cost minimization and gait plasticity *J. Exp. Biol.* **208** 979–91
[24] Bertram J E A and Ruina A 2001 Multiple walking speed–frequency relations are predicted by constrained optimization *J. Theor. Biol.* **209** 445–53
[25] Cavagna G A and Franzetti P 1986 The determinants of the step frequency in walking in humans *J. Physiol.* **373** 235–42
[26] Chandrakasan A P, Sheng S and Brodersen R W 1992 Low-power CMOS digital design *IEICE Trans. Electron.* **75** 371–82
[27] Döring J, Bovtun V, Gaal M, Bartusch J, Erhard A, Kreutzbruck M and Yakymenko Y 2012 Piezoelectric and electrostrictive effects in ferroelectret ultrasonic transducers *J. Appl. Phys.* **112** 084505
[28] Zhang X, Huang J, Wang X and Xia Z 2010 Piezoelectricity and dynamic characteristics of laminated fluorocarbon films *IEEE Trans. Dielectr. Electr. Insul.* **17** 1001–7
[29] Luo Z, Zhu D, Shi J, Beeby S, Zhang C, Proynov P and Stark B 2015 Energy harvesting study on single and multilayer ferroelectret foams under compressive force *IEEE Trans. Dielectr. Electr. Insul.* **22** 7116323
[30] Rao Y, McEachern K M and Arnold D P 2013 A compact human-powered energy harvesting system *J. Phys.: Conf. Ser.* **476** 012011
[31] Kursun V, Narendra S G, De V K and Friedman E G 2004 Low-voltage-swing monolithic dc-dc conversion *IEEE Trans. Circuits Syst. Express Briefs* **51** 241–8
[32] Yang G, Stark G B H, Hollis S J and Burrow S G Challenges for energy harvesting systems under intermittent excitation, emerging and selected topics in circuits and systems *IEEE J.* (https://doi.org/10.1109/JETCAS.2014.2337172)
[33] Chuah Y J *et al* 2015 The effects of poly(dimethylsiloxane) surface silanization on the mesenchymal stem cell fate *Biomater. Sci.* **3** 383–90